SOUTHERN JOURNAL OF SCIENCES

ESTABLISHED IN 1993

Original research paper

ADSORPTION STUDIES OF ZINC, COPPER, AND LEAD IONS FROM PHARMACEUTICAL WASTEWATER ONTO SILVER-MODIFIED CLAY ADSORBENT

AJALA, Mary Adejoke [1,2,4*]; ABDULKAREEM, Ambali Saka [2,4]; KOVO, Abdulsalami Sanni [2,4]; TIJANI, Jimoh Oladejo[3,4]; AJALA, Olawale Elijah[1]

[1] Department of Chemical Engineering, University of Ilorin, Ilorin, Kwara State, Nigeria.

[2] Department of Chemical Engineering, Federal University of Technology, Minna.

[3] Department of Chemistry, Federal University of Technology, Minna, Niger State, Nigeria.

[4] Nanotechnology Research Group, Centre for Genetic Engineering and Biotechnology (CGEB), Federal University of Technology, P.M.B 65, Bosso, Minna, Niger State, Nigeria.

** Corresponding author*
e-mail: ajala.ma@unilorin.edu.ng;

Received 12 April 2022; received in revised form 30 May 2022; accepted 14 June 2022

ABSTRACT

Background: Industrial wastewater contains pollutants that are detrimental to human health in varied proportions. Among the pollutants are heavy metals, including Zn^{2+}, $Pb^{2+,}$ and Cu^{2+} found in a characterized pharmaceutical wastewater. Several techniques have been proposed for the heavy metal sequester. However, they are with attendant challenges. The adsorption techniques using clay-metal oxide modified adsorbent/composite such as silver-clay adsorbent is considered suitable for an effective sequestering process. **Aims:** To develop and characterize Ag/clay adsorbent for pharmaceutical wastewater treatment. **Methods:** The Ag nanoparticles were synthesized using *Parkia biglobossa* aqueous leaves extract in an optimization study. The raw clay was beneficiated and doped with silver nanoparticles via the wet impregnation method. The silver-clay adsorbent was characterized using FTIR, XRD, SEM, and EDS characterization tools. The developed adsorbent was used for the batch adsorption process of the heavy metal ion removal from the wastewater. **Results and Discussion:** The phytochemical analysis and FTIR results of the *P. biglobosa* showed that the leaf contains phenol, tannin, and flavonoids which acts as reducing, capping, and stabilizing agent required for synthesizing the silver nanoparticles. The prepared silver nanoparticles modified clay adsorbent Ag/clay, have evenly distributed stacks of pseudo-hexagonal plates, are rich in silica, possess silver nanoparticles in the frameworks, and contain functional groups suitable for binding heavy metals. The adsorptions of Zn^{2+}, $Pb^{2+,}$ and Cu^{2+} from pharmaceutical wastewater onto the silver-modified clay were studied as a function of adsorbent dosage and contact time. The percentage removal results obtained showed that the adsorbent had up to 99.96%, 99.5%, and 99.44% removal efficiency for Zn^{2+}, $Pb^{2+,}$ and Cu^{2+}, respectively, which are better compared with previous studies. The adsorption process was feasible, spontaneous, and exothermic, with Langmuir and Pseudo-second-order models as best fits for the process. **Conclusions**: The adsorption of selected heavy metal ions onto the green synthesized silver-modified clay adsorbent (Ag/clay) was feasible, spontaneous, and exothermic in the order Zn^{2+}>Pb^{2+}>Cu^{2+} with Langmuir and Pseudo-second-order model best fitted for the process. These show that the synthesized silver oxide nanoparticles supported on local clay can be used as a potentially low-cost adsorbent to remove heavy metal ions from industrial wastewater.

Keywords: *Green synthesis, Parkia biglobosa, Silver oxide, Nanoadsorbent, heavy metals*.

1. INTRODUCTION

The pharmaceutical industry is a major producer of wastewater effluents containing pollutants such as heavy metals (zinc (Zn), copper (Cu), and lead (Pb)), microbes (bacteria), and dyes (yellow). The pollutants reduce the photosynthetic activity of aquatic life and could poison certain forms of aquatic life (Bashir *et al.*, 2020). Zn, Cu, and Pb ions are part of pollutants in pharmaceutical wastewater, which are hazardous and harmful to human health. Although Zn is an essential element in humans because it could serve as a food supplement, its excess is extremely dangerous as it may cause paralysis

and neurological problems. Excess Zn may also lead to a state of depression and other unwanted effects such as dizziness, breathing problems, and chest pain (Kaur and Sharma, 2017). More so, the WHO guidelines gave the maximum admissible concentration of Zn in an aqueous solution as 5.0 mg/l (WHO, 2019). Also, Cu has been reported to have adverse effects on human health. These include mental disorders, anemia, arthritis/rheumatoid arthritis, hypertension, and liver enlargement (Lakherwal, 2014). Furthermore, the WHO gave the maximum admissible concentration of Cu in an aqueous solution as 0.05 mg/l (Bankole *et al.*, 2019). On the other hand, lead is responsible for lung dysfunction, liver damage, reduced pulmonary function, and cardiovascular dysfunction (Balali-Mood, Naseri, Tahergorabi, Khazdair, and Sadeghi, 2021). Hence, Zn, Cu, and Pb removal from pharmaceutical wastewater are essential for human and aquatic survival.

Several conventional techniques such as photocatalytic oxidation, chemical coagulants, bioremediation, ion-exchange resins, reverse osmosis, membrane filtration, solvent extraction, and electrolysis have been reported for the removal of various heavy metals from wastewater (Dave and Chopda, 2014). However, they are found to be inadequate with some challenges and drawbacks, such as cost-effectiveness, disposal after use, efficiency, and lack of eco-friendliness of the technological processes (Dutta, Borah, and Puzari, 2021). Therefore the need for more research on some other methods such as adsorption.

The adsorption technique is advancing in removing heavy metals, colors, and microbes from wastewater. Since the process is highly efficient, adsorbate-specific, cost-effective, easy to handle, and eco-friendliness (Dutta *et al.*, 2021). Adebayo *et al.* (2020) (Adebayo, Adegoke, and F., 2020), however, justified the use of nanomaterial as a good adsorbent for the removal of heavy metals. Furthermore, it was reported that nanomaterials have appropriate adsorption surfaces and possess unique characteristics vis-à-vis a very high surface-area-to-volume ratio. These advantages give a tremendous driving force for diffusion, especially at high temperatures (Lakherwal, 2014).

Several nanomaterials have been used for the removal of heavy metals from wastewater, and such research includes that of Mustapha *et al.* (2019), who utilized modified kaolinite clay to remove Zinc and Chromium ions from tannery wastewater (Mustapha *et al.,* 2019). In another research, a silver-clay composite was tested for iodine-129 retention and found suitable (Sadasivam and Rao, 2016). Also, Choudhury *et al.* (2021) used Montmorillonite-silver(MMT/Ag) composite to absorb methylene blue. The outcome of the findings revealed that layered, sheet-like morphology of MMT/Ag nanocomposite was synthesized and found suitable for MB adsorption from wastewater (Choudhary *et al.*, 2021). Clay/copper/silver composite was successfully synthesized by Asamoah *et al.* (2020) (Asamoah, Yaya, Nbelayim, Annan, and Onwona-Agyeman, 2020). However, the suitability of the composite was only tested against bacterial strains and not heavy metals. Kariim *et al.* (2020) used a developed nano-adsorbent to treat pharmaceutical wastewater, focusing on removing metronidazole and levofloxacin from the wastewater (Kariim, Abdulkareem, and Abubakre, 2020).

Therefore, this study investigated the development of Ag/clay adsorbent using a green synthesis approach to remove Zn, Cu, and Pb ions from pharmaceutical wastewater. The process's isothermal, kinetics, and thermodynamic parameters were investigated for an effective sorption study of the sorbate onto the adsorbent surface.

2. MATERIALS AND METHODS

2.1. Preparation procedures

2.1.1 Beneficiation of clay

The ball clay collected from Akerebiata, Ilorin in Kwara State, Nigeria, was soaked in water for 48 h to allow the clustered clay to dissolve. It was then sieved to ease the removal of the sand particles and later allowed to sediment to get the fine particles of the clay. The fine particles obtained were sun-dried, oven-dried at 100 ℃ pulverized, and then sieved with a sieve mesh of < 0.2 µm.

2.1.2 Preparation of leaf extract

The leaves extract was prepared according to the method of Ajala *et al.*(Ajala, Abdulkareem, Tijani, and Kovo, 2022) following; fresh leaves of *Parkia biglobosa* were washed with clean water and air-dried for two weeks at room temperature

to prevent the destruction of the Thermo labile constituents present in the plant by direct sun rays. The room-dried leaves were then pulverized, and the phytochemical analysis of the plants was carried out. Next,100 mL of deionized water was added to 5g of the pulverized leaf, and the solution was then boiled at 60 ℃ for 30min to extract the reducing and stabilizing agents. Finally, the aqueous extract was filtered using a muslin cloth and filter paper (Whatman no.1). The filtrate was kept in a refrigerator for the biosynthesis of silver nanoparticles.

2.1.3 Green synthesis of silver nanoparticles

The silver nanoparticles were synthesized by adopting the method of Dhand (Dhand *et al.*, 2016). *P.biglobossa* leaves were dried and pulverized. About 5g of the pulverized leaves was added to 100 mL of deionized water, boiled at 60 ℃, and stirred continuously for 30 min using a magnetic stirrer to extract the reducing and stabilizing agents. The solution was filtered using a muslin cloth and filter paper (Whatman no.1). The varied volume of leaf extract was added to the varied volume of 1mM $AgNO_3$ solution following the data gotten from the factorial design of the Design Expert. The solution was allowed to stand for 20 minutes. The pH of the resultant solution was adjusted between pH 4 and pH 10 with either 2 M NaOH or HCl. The color change from green to brown indicates the formation of nanoparticles. The solutions were characterized using a UV-Visible spectrophotometer.

2.1.4 Silver/Clay loading procedure

Forty grams (40 g) of the beneficiated clay was weighed on an analytical balance and added to a flask containing 400 mL of 1 mM $AgNO_3$. After that, 20 mL of the *P. biglobossa* leaves extract was added under continuous stirring for a few minutes (The amount of leaf extract added was obtained from the earlier synthesis of Ag nanoparticles carried out). The flask was sealed and shaken at room temperature for 24 hours in a thermostatic water bath shaker (SHA-C). The suspension was filtered using a filter paper (Whatman no.1) and washed several times with deionized water to remove residual Ag^+ ions. The residual suspension was dried in an oven at 50 ℃ for 12 hours.

2.1.5 Characterisation of the synthesized titanium dioxide

The prepared adsorbents were characterized using; Ultraviolet-visible spectroscopy (Uv-vis), Fourier Transform Infrared spectroscopy (FTIR), X-ray diffraction (XRD), High-Resolution Scanning Electron Microscopy (HRSEM), and Electron Diffraction Spectroscopy (EDS) to determine the microstructure, morphology, chemical composition, surface area, phase structure, and optical properties of the prepared Ag/clay adsorbent.

2.2 Batch Adsorption Studies

The investigations were carried out in batches to determine the effects of contact time, adsorbent dosage, and pH to check the nature of the adsorption process. The metal ions removed from the wastewater were determined in prior physicochemical parameter investigations of the pharmaceutical wastewater in previous research (Ajala *et al.,* 2022). For the batch experiment, 25 mL of the wastewater of known concentrations was poured into Ag/clay adsorbent (0.1-0.5 g dosage) in a 100 mL flat bottom flask. The mixture was shaken at a varied time (30- 240 min) and designated temperature (30-50 ℃), the supernatant was filtered through Whatman Filter Paper No. 1, and the wastewater was analyzed using AAS. The isotherm, kinetics, and thermodynamics governing the adsorption were also determined via batch experiments. The amount of Zn^{2+}, $Pb^{2+,}$ and Cu^{2+} ions adsorbed at the time (q_t), equilibrium (q_e), and the percentage removal was calculated by the Equations 1-3:

$$q_t = \frac{(C_o - C_t)V}{m} \quad \text{(Eq. 1)}$$

$$q_e = \frac{(C_o - C_e)V}{m} \quad \text{(Eq. 2)}$$

$$\text{Removal (\%)} = \frac{C_o - C_t}{C_o} X\ 100\% \quad \text{(Eq. 3)}$$

Where C_o and C_e are the initial and the final (equilibrium) metal ion concentration ($mg \cdot L^{-1}$), V is

the water sample volume (L), m is the mass (g) of adsorbent used, C_o, C_t, and C_e are the initial, final (at a designated time) and equilibrium metal ion concentration ($mg \cdot L^{-1}$) respectively (López-Luna *et al.*, 2019).

2.2.1. Adsorption kinetic models

The kinetics of Zn^{2+}, Pb^{2+}, and Cu^2 adsorption onto Ag/clay nano adsorbent was analyzed using the pseudo-first-order (PFO) (Miyah *et al.,* 2017) and pseudo-second-order (PSO) (Ho and McKay, 1999) kinetic models. The PFO and PSO model is expressed mathematically as Equations 4 and 5:

The pseudo-first-order model:

$$\ln(q_e - q_t) = q_e - k_1 t \quad \text{(Eq. 4)}$$

The pseudo-second-order model:

$$\frac{dq_t}{dt} = k_2(q_e - q_t)^2 \quad \text{(Eq. 5)}$$

Where q_e(mg/g) = adsorbed amounts of metal ion at equilibrium, q_t(mg/g) = adsorbed amounts of each metal ion at time t (min), k_1 (min^{-1}) and k_2 (mg/g min) are the pseudo-first-order and the pseudo-second order rate constants.

2.2.2. Adsorption isotherm model

The isotherm models are employed in adsorption process analysis to investigate the distribution of adsorbate molecules at the solid/liquid interface. For the adsorption of Zn^{2+}, Pb^{2+} and Cu^2 onto Ag/clay nano adsorbent, four isotherm models, namely; Langmuir (Langmuir, 1918), Freundlich (Miyah *et al.,* 2017), Temkin (Egbosiuba *et al.*, 2019) and Dubinin–Radushkevich (D–R) (Ayawei, Ebelegi, and Wankasi, 2017; Dubinin, 1969) were applied.

The mathematical representation of the models is given by the Equations 6-9:

Langmuir isotherm;

$$\frac{C_e}{q_e} = \frac{1}{q_o K_L} + \frac{C_e}{q_o} \quad \text{(Eq. 6)}$$

Freundlich isotherm;

$$\ln q_e = \ln K_F + \frac{1}{nF} \ln C_e \quad \text{(Eq. 7)}$$

Temkin isotherm;

$$q_e = \frac{RT}{b_T} \ln A_T + \frac{RT}{b_T} \ln C_e \quad \text{(Eq. 8)}$$

D–R isotherm;

$$\ln q_e = \ln q_o - K_{ad}\varepsilon^2 \quad \text{(Eq. 9)}$$

where q_e (mg/g) is the quantity of metal ion adsorbed at equilibrium, q_m (mg/g) represents maximum adsorption capacity for monolayer coverage on the surface of the adsorbent, and C_e (mg/L) represents metal ions concentration at equilibrium. k_L (L mg^{-1}) is the Langmuir equilibrium adsorption constant. K_F (mg/g) and n_F is the Freundlich adsorption isotherm constant which denotes the adsorption capacity of the adsorbent and the heterogeneity of the adsorption process, respectively. A_T (L/g) and b_T (kJ/mol) are Temkin constants related to the heat of adsorption and maximum binding energy. T (℃) is the temperature, while R (8.314 J/mol.K) is the universal gas constant, q_{ad} and q_s are constant related to adsorption mean free energy and D–R adsorption capacity at monolayer saturation, while ε is a Polanyi potential.

2.7.3. Adsorption thermodynamics

The thermodynamics studies of Zn^{2+}, Pb^{2+}, and Cu^{2+} onto Ag/clay nano adsorbent were carried out at 30, 40, and 50 ℃, respectively. These were carried out to understand the energy changes of the process. Enthalpy change (ΔH°), Gibbs free energy change (ΔG°), and entropy change (ΔS) as the major thermodynamics parameters were evaluated using Equations 10 to 15.

$$\Delta G_{ads} = \Delta G° + RTln\ Q \quad \text{(Eq. 10)}$$

The Gibbs energy change (ΔG, kJ/mol) of the metal ion(s) adsorption process was determined by Equation 10 and analyzed using Equations 11-13 in which Q describes the quotient of reaction, which relates to the metal ion concentrations of a system that is not in equilibrium. However, at equilibrium ΔG_{ads} = 0. Hence Equation 10 is reduced to Equation 11:

$$\Delta G° = -RTln\ Kd \quad \text{(Eq. 11)}$$

$$Kd = \frac{q_e}{C_e} \quad \text{(Eq. 12)}$$

$$\ln K_d = -\frac{\Delta G^0}{RT} = \frac{\Delta S}{R} - \frac{\Delta H^0}{RT} \quad \text{(Eq. 13)}$$

Where K_d is the equilibrium parameter represented by Equation 15, the values of ΔH° and ΔS° values are obtained from the slope and intercept of the Van't Hoff plots of In K_d against 1/T (Bankole *et al.*, 2019).

2.7.4 Analysis of error

All the figures obtained from each experiment and analysis were duplicated to remove or minimize errors in the results. The constants of the isotherm and kinetics studies were determined using Origin 2019 software at a 95% confidence level. To determine the isotherm and kinetic model fitness to the experimental data in this work, the linear determination coefficient (R^2), the non-linear Chi-square test (X^2), and the sum of square error (SSE) statistical error analysis tests were performed (Ngakou, Anagho, and Ngomo, 2019). The mathematical equations are represented in Equations 14 and 15.

$$X^2 = \sum((q_{e,exp} - q_{e,cal})^2 / q_{e,cal}) \quad \text{(Eq. 14)}$$

$$SSE = \sum(q_{e,\ exp} - q_{e,cal})^2 \quad \text{(Eq. 15)}$$

3. RESULTS AND DISCUSSION

3.1 Characterization result

3.1.1 FTIR of Parkia Biglobosa, Clay and Ag-clay

The structural exposition and macromolecules of *Parkia biglobosa* were evaluated using the FTIR technique (Figure 1), and the FTIR spectra showed characteristic peaks of hydrogen-bonded O-H stretch at 3533.71, 3417.98, 3363.97, and 3271.38 cm^{-1}, the peak at 3055.35 cm^{-1} indicates C=C-H asymmetric stretch. The peaks at 3417.98, 3363.97, 3271.38, and 3055.35 cm^{-1} also indicate N-H stretch. Peaks of H-C-H asymmetric and symmetric stretch were shown at 2924.18 and 2862.46 cm^{-1}, while 2746.73 cm^{-1} indicates C-H stretch off C=O; the peak at 2345.52 cm^{-1} is a result of C≡N stretch. The peaks at 1728.28 and 1627.97 cm^{-1} indicate C=O stretch; 1535.39 and 1442.80 cm^{-1} are due to H-C-H bend and C-C=C asymmetric stretch. The peaks at 1373.36, 1327.07, and 1026.16 cm^{-1} indicate the C-O stretch. The presence of the O-H stretch, which is related to phenol, serves as a reducing and stabilizing agent in the formation of the silver nanoparticles.

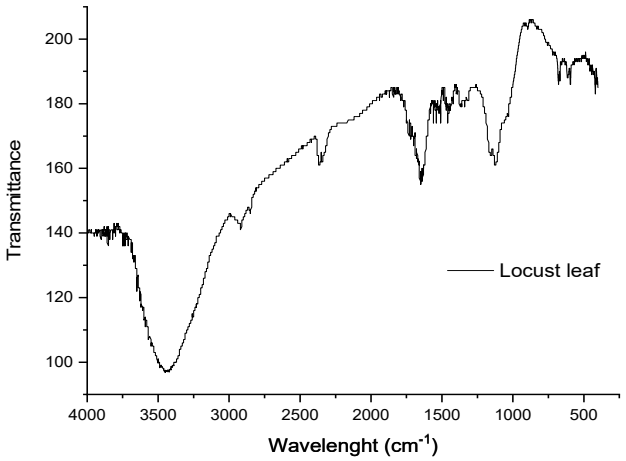

Figure 1. FTIR spectrum of Parkia biglobosa

The Fourier transform infrared (FTIR) spectroscopy of the clay was evaluated, as shown in Figure 2a. The characteristic peaks at 3701.70 and 3615.89 cm^{-1} represent the O-H stretch of alcohols and phenolic group, the peak at 1111.01cm^{-1} represents the C-O stretch of esters, while the C-O stretching peak at 1004.77cm^{-1} is of ethers. The peaks at 914.87, 792.28, and 706.47cm^{-1} are attributed to the silicate clay's Si-

O-Si and Al-O-Si bonds. The FTIR spectra of the silver clay in Figure 2b shows several peaks indicating the functional groups embedded in the adsorbent. The characteristic peak of hydrogen-bonded O-H stretch, at 3305.86 cm^{-1} is that of the phenolic and alcohol group. Bonded O-H of carboxylic acids is observed at 2928 cm^{-1}, and the peaks at 1621 and 1600 are attributed to the C=O stretch of carbonyl and ketones. Other peaks at 1298 cm^{-1}, 1251 $cm^{-1,}$ and 1186 cm^{-1} depict C-O stretch attributed to esters and ethers, indicating a shift from the previously observed in unmodified clay likely due to the chemical modification (Dhand *et al.*, 2016). Si-O-Si and Al-O-Si bonds of silicate clay are at 910 cm^{-1}, 800.24 $cm^{-1,}$ and 700 cm^{-1}. New peaks, which deviated entirely from those on the clay spectral, are observed at 534.78 cm^{-1}, 462.34 cm^{-1}, and 432.66 cm^{-1} are attributed to Ag loading, similar to the findings of Krishnan and Mahalingam (2017).

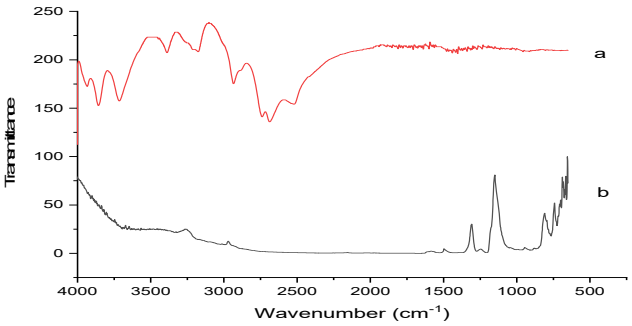

Figure 2. FTIR spectrum of (a) Raw clay and (b) Ag/clay Adsorbent

3.1.2 XRD results

The XRD result of the raw clay and Ag/clay are presented in Figures 3 (a) and (b). The diffraction pattern illustrates the presence of major peaks at 2Θ values and crystal planes at 12.31° (001), 19.80° (020), 35.92° (002), and 73.53° (-261), corresponding to the kaolinite (**k**) clay mineral peaks which agrees with the JCP library01-079-1570. Silicon oxide in the form of quartz (q) was observed at 20.91° (100), 26.80° (101), 40.22° (111), and 60.01° (211), 67.60°(212), 73.77°(014) (JCP-01-083-0539) (Ajala *et al.*, 2022), while the scanty short peaks at 24.94°, 28.56° are Albite (**a**) ($Na1.09(Al1.09Si2.91O8)$) peaks. The Microcline (**m**) peaks in Figure 3(b) are the transformations of the kaolinites due to hydrolysis. Other peaks are at 76.42° and 82.02°, synchronized to calcite-magnesian peaks (**c**) ($MgO.CaO.CO_3$) as impurities in the clay source. The calcite peaks in Figure 3(a) were observed absent in Figure 3(b), this is attributed to the beneficiation and modification processes carried out on the clay. The presence of high-intensity peaks in Figure 3(a) was reduced to low intensity in Figure 3(b), and there was the total disappearance of the calcite peaks earlier observed in Figure 3(a). This improvement suggests that the immobilization of the silver nanoparticles in the clay surface has led to the changes observed. This agrees with previous literature (Alaya-Ibrahim, Kovo, Abdulkareem, Adeniyi, and Yahya, 2019).

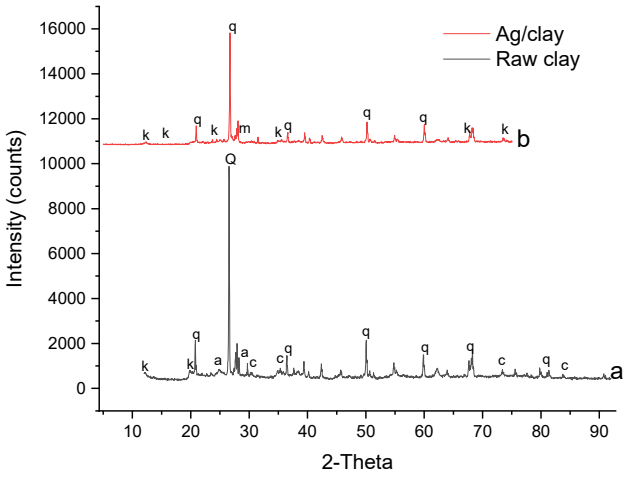

Figure 3. XRD of the Silver/clay Adsorbent

3.1.3 Morphology and Structure

The Scanning Electron Microscope was used to examine the surface morphology of the prepared adsorbent. Figure 4 reveals an evenly distributed arrangement of spherical nanocomposites. The flat-lying stacks are pseudo-hexagonal in a structure having curved edges, which are the characteristics of kaolinite clays. The even arrangement may imply polydispersity and intercalation of the silver nanoparticles into the clay structure. The EDS result in Figure 5 shows that the clay is truly rich in silica at 24.9%, bonded oxygen is up to 48.68% of the entire weight, and titanium and iron elements have low weight percent of 0.46 and 2.39%, respectively. After the beneficiation process and reduction of silver nanoparticles into the clay, the percentage weight of silicon in the Ag/clay became 13.97%, Aluminium, 11.71%, which further revealed the kaolinite nature of the clay (Al: Si equals 1:1). The EDS result also confirmed the successful immobilization of the silver nanoparticles on the clay with 0.74% of Ag present in the prepared adsorbent. Ti and Fe were also retained on the

Ag/clay composite at reduced percentages compared to the unmodified clay.

3.2. Adsorption studies

3.3.1 Effect of contact time on the removal of the heavy metals using silver-clay adsorbent

The influence of contact time on the removal of Zn^{2+}, $Pb^{2+,}$ and Cu^{2+} ions was studied between 30 to 240 min, keeping other parameters constant (Temperature; 30 ℃, dosage; 0.5 g, concentration; 100mg/L, pH; 7). Figure 6 shows the effect of contact time on the adsorption of Zn^{2+}, $Pb^{2+,}$ and Cu^{2+} ions. From the figure, as the adsorption time increased from 30 to 240 min, the percentage removal of the metal ion (Zn^{2+}, $Pb^{2+,}$ and Cu^{2+}) increased. Arising steadily from 92.3%, 81.2%, and 80.1% at 30 min to 97.82%, 85.83%, and 85.39% at 90 min, respectively, remained constant afterward. Rapid metal ion uptake of the metal ion may be linked to available surface adsorption sites on the Ag-clay adsorbent (Adebayo, Adegoke, and Sidiq, 2020). Equilibrium was attained at 90 min of the adsorption process, linked to the surface coverage of the adsorbent per time and adherence to functional groups on the adsorbent until no further adsorption occurs.

3.3.2 Effect of adsorbent dose on the removal of the heavy metals

The effect of adsorbent dosage on Zn^{2+}, $Pb^{2+,}$ and Cu^{2+} removal from the wastewater was investigated, and the results are presented in Figure 7. From the figure, increasing the amount of adsorbent from 0.1 g to 0.3 g increases Zn^{2+}, Pb^{2+} and Cu^{2+} percentage removal from the aqueous solution. However, there was no further increment in the percentage adsorbed beyond 0.3 g, as shown in Figure 7. This is because there is no more exposure of the metal ion to the available binding sites due to small adsorbate in the medium, causing less metal ion per gram adsorption (Ajala *et al.*, 2022). In addition, with the increase in adsorbent dosage, aggregation of particles occurs due to the low volume of solution, and as a result, removal efficiency and adsorption of Zn^{2+}, $Pb^{2+,}$ and Cu^{2+} decreases.

3.3.3 Effect of pH on the removal of the heavy metals

In the adsorption process of metal ions from aqueous solutions, the pH of the solution plays an important role. It is apparent from the results represented in Figure 8 that, with the increase in pH, the adsorption of metals increased gradually. Maximum adsorption (99.94%, 99.55, and 99.44% for Zn^{2+}, $Pb^{2+,}$ and Cu^{2+}, respectively) was observed between pH 7 and pH 10, while adsorption of the metal ions was inhibited at lower pH (2–6). The Maximum removal efficiency obtained at high pH was because deprotonation takes place due to the presence of too many OH^- ions produced in the solution, making the surface of Ag/clay become negatively charged. (Hajjaji *et al.*, 2018). Also, higher pH may have improved the electrostatic interaction between negatively charged adsorbent surface and heavy metal ions, which are positively charged, boosting the adsorption of Zn^{2+}, Pb^{2+} and Cu^{2+} onto Ag-Clay composites. Hence the removal efficiency increases with an increase in pH.

3.3.4 Effect of temperature on the removal of the heavy metals

The solution temperature plays a vital role in the adsorption of Zn^{2+}, $Pb^{2+,}$ and Cu^{2+} metal ions onto Ag-clay, as presented in Figure 9. The percentage removal of the three ions was found to increase with the increase in the solution temperature. The adsorption rate of Zn^{2+}, Pb^{2+}, and Cu^{2+} by the Ag-clay nanocomposite rapidly reached a maximum of 97.00%, 88.50%, and 88.33%, respectively, at 40 ℃ as shown in Figure 9. This phenomenon indicates that the adsorption process of the metal ions onto the nanoparticles may be described as chemisorption or process (Bankole *et al.,* 2019). It can be explained that, at the temperature of 40 ℃, the activation of the adsorbent surfaces is enlarged, facilitating more active sites for the adsorption of the metal ions. Moreover, easy mobility and enhanced accessibility of metal ions from the bulk solution to the adsorbent active sites could also be the reason for the maximum adsorption of metal ions at higher temperatures. Also, from the obtained graph, the adsorption for Zn^{2+}, $Pb^{2+,}$ and Cu^{2+} was not so favorable at a temperature higher than 40 ℃ for the Cu^{2+} ion. Therefore, optimum multi-ion adsorption may not go beyond 40 ℃ temperature.

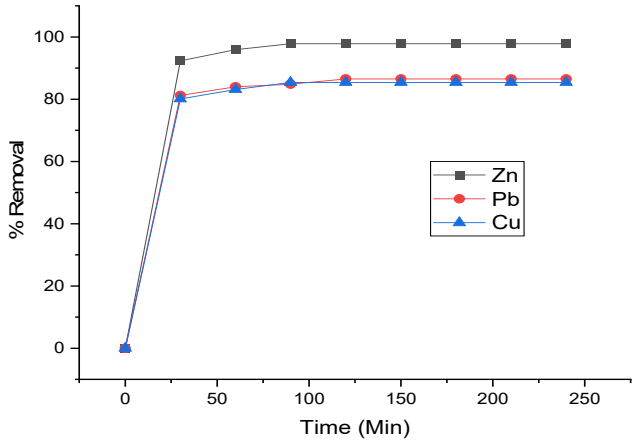

Figure 6. Effect of contact time on % removal

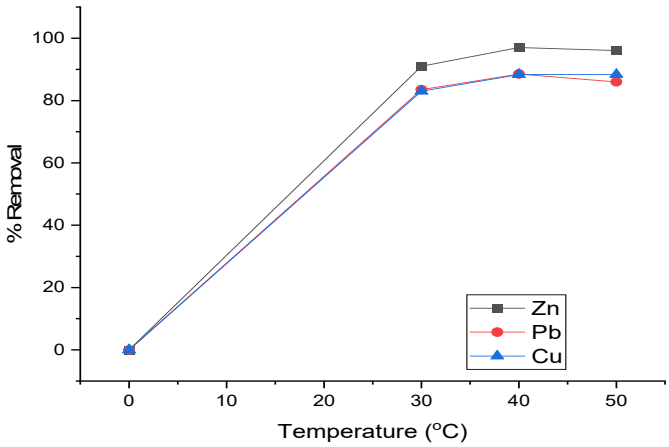

Figure 9. Effect of Temperature on % removal

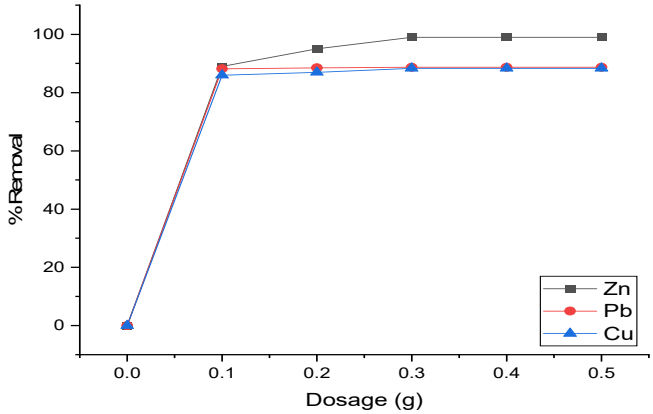

Figure 7. Effect of adsorbent dosage on % removal

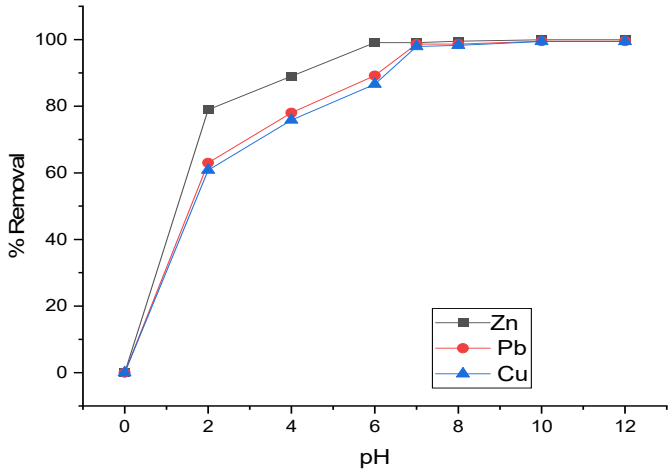

Figure 8. Effect of pH on % removal

3.4 Adsorption Isotherm Studies

The equilibrium adsorption isotherms are essential data sources to design, understand, and optimize the adsorption process. The data expresses the intrinsic properties and interaction between adsorbate and adsorbent. The data can be used to compare the adsorptive capacities of the adsorbent for different pollutants. Isotherm models investigated for the adsorption of Zn^{2+}, $Pb^{2+,}$ and Cu^{2+} onto Ag/Clay are; Langmuir, Freundlich, Temkin, and Dubinin–Radushkevich, and the result is presented in Table 1. From the table, the Langmuir isotherm has the correlation coefficients (R^2) of 0.976, 0.994, and 0.964 for Zn^{2+}, $Pb^{2+,}$ and Cu^2 respectively, which are the highest of the four isotherm models tested. The results show that the Langmuir model is suitable to explain the sorption behavior of the adsorption of the heavy metal ions onto the prepared adsorbent. The Langmuir theory (Langmuir 1918) suggests that the sorbent surface is homogeneous, and there is no interaction in-between the molecules adsorbed during the formation of a monolayer surface coverage. The R_L value calculated for the three ions is between 8.162×10^{-5} and 3.110×10^{-4}, which are less than 1. These values suggest that the adsorption of the ions onto the adsorbents was favorable in all the conditions investigated. Also, from Table 1, the magnitude of the Freundlich isotherm constant K_F suggests that the sorption capacity of the experimented metal ions was in $Zn^{2+} < Cu^{2+} < Pb^{2+}$ order. The value of $N_F > 1$ for Zn^{2+}, Cu^{2+} and Pb^{2+} suggest heterogeneity of the adsorbent surface, and that the metal ions are favorably and intensively adsorbed by silver clay under the experimental conditions. Temkin isotherm constant (b_T), otherwise known as the equilibrium binding factor, was calculated from the Temkin

isotherm expression and shown in Table 1. As shown in Table 1, Pb^{2+} has the highest equilibrium binding constant at low temperatures. The low values of the Temkin adsorption potential, A_T in the range of 3.418 to 0.115 (L/mg), indicate a lower sorbent-metal ion potential. The Dubinin–Radushkevich (D-R) isotherm was applied to distinguish the physical and chemical adsorption of metal ions with its mean free energy. The D-R isotherm has the lowest regression values plots are 0.891, 0.443, and 0.651 for Zn^{2+}, Pb^{2+}, and Cu^{2+}, respectively. The apparent free energy (E) values obtained less than (<) 40 kJ/mol, which signifies that the nature of the adsorption mechanism is physisorption (Ayawei *et al.,* 2017). Comparing the average error functions (X^2 and SSE), it was reported that the closer to zero the values of the error functions are, the suitability of the model reported (Egbosiuba *et al.,* 2020). Therefore from Table 1, out of the four isotherms, the Langmuir isotherm has the lowest error values, which are closer to zero than those of the Freundlich, Temkin, and Dubinin–Radushkevich isotherms. These results further confirmed the suitability of the Langmuir isotherm model for the description of the adsorption process, which means; the adsorption of Zn^{2+}, Cu^{2+} and Pb^{2+} is based on single-layer coverage on the adsorbent surface which depicts a monolayer formation.

3.5 Adsorption Kinetics Studies

The kinetic data are essential to understanding the rate and nature of adsorption onto the adsorbents. In addition, the data can be used to compare the kinetics of the adsorbent for different pollutants. Figures 10 and 11 show the Pseudo-first-order (PFO) and Pseudo-second-order (PSO) plots for the adsorption of Zn^{2+}, Pb^{2+}, and Cu^{2+} onto the Ag/clay adsorbent from which the kinetics parameters in Table 2 was obtained. The PFO is based on multi-layer adsorption on the adsorbent surface, explained by the forces such as the Van der Waals (Ngakou *et al.,* 2019). From the table, the regression coefficients (R^2) for the heavy metal ions are 0.839, 0.917, and 0.935 for the PFO. This result suggests that the experimental data support the PFO model to describe adsorption kinetics of the three metal ions, most especially for Cu^{2+}.

However, the differences between the modeled adsorptive capacity values, ($q_{e,\ cal}$) and the experimental values ($q_{e,\ exp}$) are very high. This refers to the fact that both the metal ions and adsorbents were involved in the adsorption process (Meitei and Prasad, 2014). Therefore, from the residual plot and the error functions, it is suggested that the pseudo-first-order model does not describe the kinetic sorption of the process sufficiently, over the range of experimental time considered. Also from Table 2 presented, it was noted that the regression coefficients for the three ions are high in the order; Cu^{2+} (0.982) > Pb^{2+} (0.969) > Zn^{2+} (0.968) which implies good correlation of the model. Considering the modeled and the experimental values of the adsorptive capacities ($q_{e,\ cal,}$ and $q_{e,\ exp}$), the obtained values are closer unlike that of the PFO that are wide apart. Moreover, the error function values (SSE and X^2) for PSO are lower compared with the PFO. This suggests that the PSO kinetic model fits the adsorption process better. This interaction implies that there is a mono-layer coverage between the adsorbed and the adsorbent, with π-π bond interactions as the major bonds formed (Bello, Chris, Oluwakemi, and Olatunde, 2020; Ngakou *et al.*, 2019) in the Zn^{2+}, Pb^{2+}, and Cu^{2+} adsorption onto the Ag/clay surface.

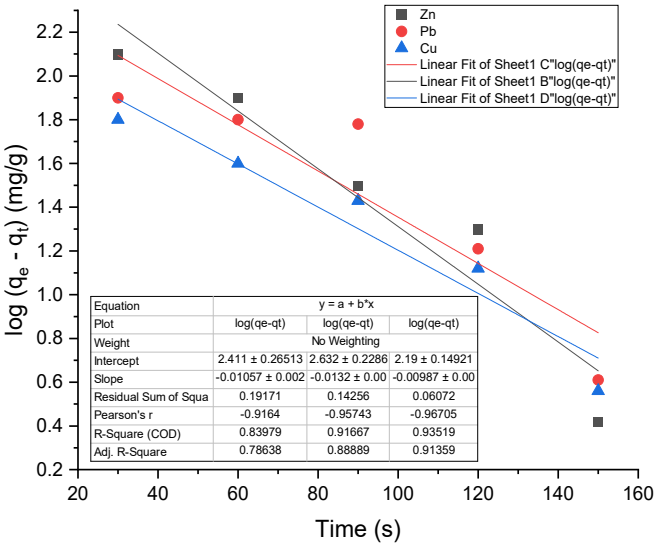

Figure 10. Pseudo-first-order plots

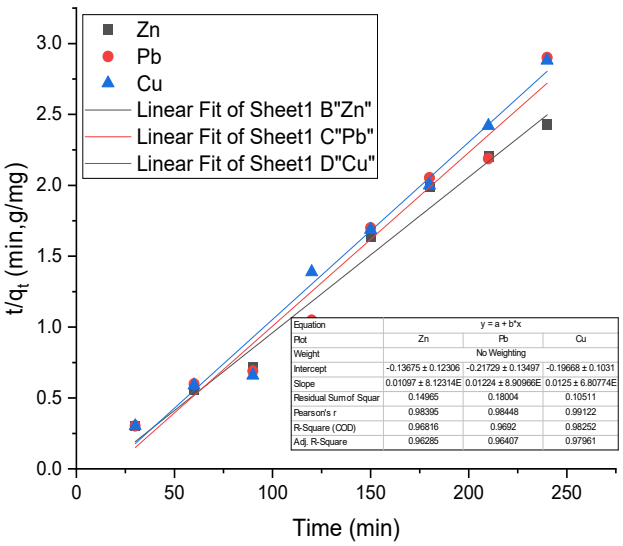

Figure 11. Pseudo-second-order plots

To justify the Zn^{2+}, Pb^{2+}, and Cu^{2+} adsorption from pharmaceutical wastewater, the results obtained in this study were compared with the percentage removal of pollutants by other adsorbents. The result of the findings for another pollutant removal by silver and clay-formulated adsorbents is presented in Table 3. The data in Table 3 showed that the percentage removal of Zn^{2+}, Pb^{2+} and Cu^{2+} ions using the Ag/clay adsorbent was higher than that of acid-activated Bentonite clay for the removal of similar heavy metal ions (Budsaereechai, Kamwialisak, and Ngernyen, 2012). In another research where Ag/kaolinite was used to remove an Acid cyanine dye, about 90% removal percentage of the dye was reported (Hashemian and Shahedi, 2013). Other composites/adsorbents such as AgNPs/TAC (Trinh *et al.*, 2020), Ag/TiO_2 (Demirci *et al.*, 2016), Clay/ZnO/Ag (Demirci *et al.*, 2016) do not compare efficiently with the 99.96%, 99.5%, and 99.44% removal efficiency obtained for Zn^{2+}, Pb^{2+}, and Cu^{2+} in the present study. This indicated that Ag/clay is a potentially effective and efficient adsorbent for removing heavy metal ions from aqueous solutions.

3.6. Thermodynamics

The adsorption thermodynamics was fitted by Vant Hoff's linear plot of ln K_d versus 1/T in Figure 12. From the figure, thermodynamics parameters; Gibb's free energy (ΔG°), enthalpy (ΔH°), and entropy (ΔS°) values were obtained as shown in Table 4. The negative Gibb's free energy (ΔG°) value obtained for the three ions at various temperatures revealed the adsorption of Zn^{2+}, Pb^{2+}, and Cu^{2+} ions onto Ag/clay adsorbents was feasible and spontaneous. The obtained ΔH° values at 313, 323, and 333 K temperatures are negative, this shows that the adsorption process is exothermic. Also in Table 4, the enthalpy values obtained for Zn^{2+}, and Cu^{2} (II) were greater than 40 kJ/mol, suggesting that the process is more chemically controlled than physically controlled, similar to previous research (Khulbe and Matsuura, 2019). The negative ΔS° implied that there is a reduction in the degree of randomness at the Ag/clay and Zn^{2+}, Pb^{2+}, and Cu^{2+} interfaces during the sorption process.

4. CONCLUSIONS

A new adsorbent was synthesized using local clay from Akerebiata, Ilorin modified with silver nanoparticles. The synthesis of Ag nanoparticles in a green process confirms the suitability of *Parkia biglobosa* leaf extract as a reducing, capping, and stabilizing agent. The local clay was also confirmed kaolinite in nature, rich in silica, and contains functional groups capable of binding metal ions to themselves. The adsorption of selected heavy metal ions; Zn^{2+}, Pb^{2+}, and Cu^{2+} onto the silver-modified clay was affected by contact time, pH, adsorbent dosage and temperature with equilibrium attained at 90 min. The Langmuir isotherm and Pseudo-second-order kinetics model best modeled the adsorption process. It was feasible, spontaneous, and exothermic in the order Zn^{2+}>Pb^{2+}>Cu^{2+}. The silver-clay adsorbent is, therefore, suitable and efficient for removing heavy metal ions from an aqueous solution.

5. DECLARATIONS

5.1. Study Limitations

No limitations were known at the time of the study.

5.2. Acknowledgements

The authors would like to thank the University of Ilorin, Ilorin Nigeria for providing enabling environment for this research.

5.3. Funding source

The authors funded this research.

5.4. Competing Interests

No potential conflict of interest exists in this publication.

6. REFERENCES:

1. Adebayo, G. B., Adegoke, H. I., and F., S. (2020). Adsorption of Cr(VI) ions onto goethite, activated carbon and their composite: kinetic and thermodynamic studies. *Applied Water Science, 10*, 213-231. doi:10.1007/s13201-020-01295-z
2. Adebayo, G. B., Adegoke, H. I., and Sidiq, F. (2020). Adsorption of Cr(VI) ions onto goethite, activated carbon and their composite: kinetic and thermodynamic studies. *Applied Water Science, 10*, 213-231. doi:10.1007/s13201-020-01295-z
3. Ajala, M. A., Abdulkareem, A. S., Tijani, J. O., and Kovo, A. S. (2022). Adsorptive behaviour of rutile phased titania nanoparticles supported on acid-modifed kaolinite clay for the removal of selected heavy metal ions from mining wastewater. *Applied Water Science, 12*(19), 1-24. doi:10.1007/s13201-021-01561-8
4. Ajala, M. A., Ajala, E. O., Tayo-Alabi, A., Sodiq, H. K., Abdulkareem, A. S., Kovo, A. S., and Tijani, J. O. (2022). Development of Titanium Dioxide Pillared Clay Adsorbent for Removal of Lead (II), Zinc (II), and Copper (II) ions from Aqueous Solution. *UNIOSUN Journal of Engineering and Environmental Sciences, 4*(1), 264-280. doi:10.36108/ujees/2202.40.0172
5. Alaya-Ibrahim, S., Kovo, A. S., Abdulkareem, A. S., Adeniyi, O. D., and Yahya, M. D. (2019). Development of nano-silver doped zeolite Asynthesized from Nigerian Ahoko kaolin for treatment of wastewater of a typical textile company. *Chemical Engineering Communications, 9*, 1-25. doi:10.1080/00986445.2019.1641490
6. Asamoah, R. B., Yaya, A., Nbelayim, P., Annan, E., and Onwona-Agyeman, B. (2020). Development and Characterization of Clay-Nanocomposites for Water Purification. *Materials (Basel, Switzerland), 13*(17), 3793. doi:10.3390/ma13173793
7. Ayawei, N., Ebelegi, A. N., and Wankasi, D. (2017). Modelling and Interpretation of Adsorption Isotherms. *Journal of Chemistry, 2017*, 3039817. doi:10.1155/2017/3039817
8. Balali-Mood, M., Naseri, K., Tahergorabi, Z., Khazdair, M. R., and Sadeghi, M. (2021). Toxic Mechanisms of Five Heavy Metals: Mercury, Lead, Chromium, Cadmium, and Arsenic. *12*(227). doi:10.3389/fphar.2021.643972
9. Bankole, M. T., Abdulkareem, A. S., Mohammed, I. A., Ochigbo, S. S., Tijani, J. O., Abubakre, O. K., and Roos, W. D. (2019). Selected heavymetals removal from electroplating wastewater by purifiedand polyhydroxylbutyrate functionalized carbon nanotubesadsorbents. . *Scientific Report, 9*, 1-19. doi:10.1038/s41598-018-37899-4
10. Bashir, I., Lone, F. A., Bhat, R. A., Mir, S. A., Dar, Z. A., and Dar, S. A. (2020). Concerns and Threats of Contamination on Aquatic Ecosystems. In K. R. Hakeem, R. A. Bhat, and H. Qadri (Eds.), *Bioremediation and Biotechnology: Sustainable Approaches to Pollution Degradation* (pp. 1-26). Cham: Springer International Publishing.
11. Bello, O., Chris, T., Oluwakemi, C. A., and Olatunde, A. (2020). Sequestering a non-steroidal anti-inflammatory drug using modified orange peels. *Applied Water Science, 10*. doi:10.1007/s13201-020-01254-8
12. Budsaereechai, S., Kamwialisak, K., and Ngernyen, Y. (2012). Adsorption of lead, cadmium and copper on natural and acid activated bentonite clay. *KKU Research*

Journal, 17(5), 800-810.

13. Choudhary, N., Yadav, V. K., Yadav, K. K., Almohana, A. I., Almojil, S. F., Gnanamoorthy, G., . . . Jeon, B. H. (2021). Application of Green Synthesized MMT/Ag Nanocomposite for Removal of Methylene Blue from Aqueous Solution. *Water, 13*(3206). doi:10.3390/w13223206
14. Dave, P., and Chopda, L. (2014). Application of Iron Oxide Nanomaterials for the Removal of Heavy Metals. *Journal of Nanotechnology, 2014*(1), 1-14. doi:10.1155/2014/398569
15. Demirci, S., Dikici, T., Yurddaskal, M., Gultekin, S., Toparli, M., and Celik, E. (2016). Synthesis and characterization of Ag doped TiO2 heterojunction films and their photocatalytic performances. *Applied Surface Science, 390*, 591-601. doi:https://doi.org/10.1016/j.apsusc.2016.08.145
16. Dhand, V., Soumya, L., Bharadwaj, S. G., Chakra, S., Bhatt, D., and Sreedhar, B. (2016). Green synthesis of silver nanoparticles using Coffea arabica seed extract and its antibacterial activity. *Materials science and engineering. C, Materials for biological applications, 58*, 36-43. doi:10.1016/j.msec.2015.08.018
17. Dubinin, M. M., 1969. (1969). The potential theory of adsorption of gastheory of adsorption of gases and vapour. *Chem. Rev., 60*, 235-241
18. Dutta, D., Borah, P. J., and Puzari, A. (2021). Iron oxide coated hollow poly(methylmethacrylate) as an efficient adsorption media for removal of arsenic from water. *RSC Advances, 11*, 13376-13385. doi:10.1039/D0RA10801D
19. Egbosiuba, T. C., Abdulkareem, A. S., Kovo, A. S., Afolabi, E. A., Tijani, J. O., Auta, M., and Roos, W. D. (2019). Ultrasonic enhanced adsorption of methylene blue onto the optimized surface area of activated carbon: Adsorption isotherm, kinetics and thermodynamics. *Chemical Engineering Research and Design, 153*, 315-336. doi:10.106/j.cherd.2019.10.016
20. Egbosiuba, T. C., Abdulkareem, A. S., Kovo, A. S., Afolabi, E. A., Tijani, J. O., and Roos, W. D. (2020). Enhanced adsorption of As(V) and Mn(VII) from industrial wastewater using multi-walled carbon nanotubes and carboxylated multi-walled carbon nanotubes. *Chemosphere, 254*(126780). doi:10.1016/j.chemosphere.2020.126780
21. Hajjaji, W., Andrejkovičová, S., Pullar, R. C., Tobaldi, D. M., Lopez-Galindo, A., Jammousi, F. and Labrincha, J. A. (2018). Effective removal of anionic and cationic dyes by kaolinite and TiO2/kaolinite composites. *Clay Minerals, 51*(1), 19-27. doi:10.1180/claymin.2016.051.1.02
22. Hashemian, S., and Shahedi, M. R. (2013). Novel Ag/Kaolin Nanocomposite as Adsorbent for Removal of Acid Cyanine 5R from Aqueous Solution. *Journal of Chemistry, 2013*, 285671. doi:10.1155/2013/285671
23. Ho, Y. S., and McKay, G. (1999). Pseudo-second order model for sorption processes. 34, 451–465. *Process Biochemistry, 34*(5), 451-465. doi:10.1016/S0032-9592(98)00112-5
24. Kariim, I., Abdulkareem, A. S., and Abubakre, O. K. (2020). Development and characterization of MWCNTs from activated carbon as adsorbent for metronidazole and levofloxacin sorption from pharmaceutical wastewater: Kinetics, isotherms and thermodynamic studies. *Scientific African, 7*(2020). doi:10.1016/j.sciaf.2019.e00242
25. Kaur, A., and Sharma, S. (2017). Removal of Heavy Metals from Waste Water by using Various Adsorbents- A Review. *Indian Journal of Science and Technology, Vol 10(34), DOI: , September 2017, 10*(34). doi:10.17485/ijst/2017/v10i34/117269
26. Khulbe, K. C., and Matsuura, T. (2019). Removal of heavy metals and pollutants by membrane adsorption techniques. *Applied Water Science, 8*(19), 1-30. doi:10.1007/s13201-018-0661-6
27. Korolkova, S. V., Volovicheva, N. A., Vezentsev, A. I., Gorbunova, N. M., and Nurasyl, T. E. (2020). Sorption of Cu^{2+} ions and Fe^{3+} with alkaline forms of montmorillonite containing clay. *European Journal of Molecular and Clinical Medicine, 7*(2), 5586-5597
28. Lakherwal, D. (2014). Adsorption of Heavy Metals: A Review. *International Journal of Environmental Research and Development. , 4*(1), 41-48

29. Langmuir, I. (1918). The Constitution and Fundamental properties of Solids and Liquids. *Journal of American Chemical society., 38*, 2221-2295

30. López-Luna, J., Ramírez-Montes, L. E., Martinez-Vargas, S., Martínez, A. I., Mijangos-Ricardez, O. F., González-Chávez, M. A., . . . Vázquez-Hipólito, V. (2019). Linear and nonlinear kinetic and isotherm adsorption models for arsenic removal by manganese ferrite nanoparticles. *SN Applied Sciences, 1*(950), 1-19. doi:10.1007/s42452-019-0977-3

31. Meitei, M. D., and Prasad, M. N. V. (2014). Adsorption of Cu (II), Mn (II) and Zn (II) by Spirodela polyrhiza (L.): Equilibrium, Kinetic and Thermodynamic studies *Ecological Engineering, 71*, 308–317

32. Miyah, Y., Lahrichi, A., Idrissi, M., Boujraf, S., Taouda, H., and Zerrouq, F. (2017). Assessment of adsorption kinetics for removal potential of Crystal Violet dye from aqueous solutions using Moroccan pyrophyllite. *Journal of the Association of Arab Universities for Basic and Applied Sciences, 23*, 20-28. doi:10.1016/j.jaubas.2016.06.001

33. Mustapha, S., Ndamitso, M. M., Abdulkareem, A. S., Tijani, J. O., Mohammed, A. K., and Shuaib, D. T. (2019). Potential of using kaolin as a natural adsorbent for the removal of pollutants from tannery wastewater. *Heliyon, 5*(e02923), 1-17. doi:10.1016/j.heliyon.2019.e02923

34. Ngakou, C. S., Anagho, G. S., and Ngomo, H. M. (2019). Non-linear Regression Analysis for the Adsorption Kinetics and Equilibrium Isotherm of Phenacetin onto Activated Carbons. *Current Journal of Applied Science and Technology, 36*(4), 1-18

35. Sadasivam, S., and Rao, S. (2016). Characterization of silver—kaolinite (AgK): An adsorbent for long–lived 129I species. *SpringerPlus, 5*. doi:10.1186/s40064-016-1855-8

36. Trinh, V. T., Nguyen, T. M., Van, H. T., Hoang, L. P., Nguyen, T. V., Ha, L. T., . . . Nguyen, X. C. (2020). Phosphate Adsorption by Silver Nanoparticles-Loaded Activated Carbon derived from Tea Residue. *Scientific Reports, 10*(3634), 1-13. doi:10.1038/s41598-020-60542-0

37. WHO. (2019). WHO Guidelines for Drinking Water Quality: First Addendum to the Fourth Edition. In J. A. Cotruvo (Ed.), (Vol. 109, pp. 44-51). Washington, DC, USA: American Water Works Association.

***Table 1.**: Adsorption isotherm model parameters for the metal ion adsorption onto silver oxide nanoparticles modified clay*

Model	**Parameter**	**Metal ions**		
		Zn^{2+}	**Pb^{2+}**	**Cu^{2+}**
Langmuir	q_m (mg/g)	10.030	22.222	6.803
	K_L	1.231	3.214	12.250
	R_L	$8.117x10^{-4}$	$3.110x10^{-4}$	$8.162x10^{-5}$
	R^2	0.980	0.973	0.960
	X^2	0.003	$6.85x10^{-6}$	$4.725x10^{-5}$
	SSE	0.012	$2.73x10^{-5}$	$1.890x10^{-4}$
Freundlich	K_F (mg/g)	0.509	1.000	1.000
	N	1.56	0.651	1.073
	R^2	0.955	0.933	0.916
	X^2	0.006	0.049	0.023
	SSE	0.022	0.194	0.091
Temkin	A_T (L/g)	0.115	3.418	0.627
	b_T (kJ/mol)	0.126	0.180	0.097

	R^2	0.815	0.611	0.843
	X^2	128.647	445.907	178.410
	SSE	514.587	8.842	713.640
D-R	E(kJ/mol)	0.354	0.354	0.360
	K_{ad}	3.977	3.982	3.867
	R^2	0.892	0.443	0.651
	X^2	0.071	0.515	0.208
	SSE	0.285	2.060	0.813

Table 2. *Kinetics parameter of the metal ions adsorption onto Ag/clay adsorbent*

Model	**Parameter**	**Metal ions**		
		Zn^{2+}	**Pb^{2+}**	**Cu^{2+}**
PFO	$q_{e,exp}$ (mg/g)	97.800	97.000	96.400
	$q_{e,cal}$ (mg/g)	11.145	13.902	8.935
	k_1 (min^{-1})	0.011	0.013	0.010
	R^2	0.839	0.917	0.935
	SSE	0.192	0.143	0.061
	X^2	0.064	0.048	0.020
PSO	$q_{e,exp}$ (mg/g)	97.800	97.000	96.400
	$q_{e,cal}$ (mg/g)	90.910	83.330	76.92
	k_2 (min^{-1})	0.001	0.001	0.002
	R^2	0.968	0.969	0.982
	SSE	0.149	0.108	0.011
	X^2	0.024	0.030	0.018

Table 3. *Comparison of Ag/clay removal capacity with other adsorbents for pollutants removal*

Adsorbent	**Pollutants removed**	**Adsorptive conditions**	**Removal capacity %**	**Reference**
Acid activated bentonite clay	Cu^{2+}, Cd^{2+} and Pb^{2+}	t=36 h, Co =2000 mg/L, d=1g	36.68, 57.88, 92.85%	Budsaereechai *et al.* (2012)
Montmorillonite clay	$Cu^{2+,}$ Fe^{3+}	t=42 h, T=25ºC, d=2g	0.358, 0.189 mmol/g	Korolkova, Volovicheva, Vezentsev, Gorbunova, and Nurasyl (2020)
Kaolin	Methylene blue	t=20 min	90%	Hajjaji *et al.* (2018)
Ag/kaolin nanocomposite	Acid cyanine dye	pH 3, t=60 min	90%	Hashemian and Shahedi (2013)
AgNPs/TAC	Phosphate	pH 3, t=150 min, Co=30 mg/L	78.0% (13.62 mg/g)	Trinh *et al.* (2020)
Clay/CuO/Ag	*E. coli*	t=48 h	90%	Asamoah *et al.* (2020)
Clay/ZnO/Ag	*S. aureus*	t=48 h	>90%	Asamoah *et al.* (2020)

Ag/TiO_2	Methylene blue	Co=3 mg/L	54.13%	Demirci *et al.* (2016)
Ag/clay	Zn^{2+}, Pb^{2+}, and Cu^{2+}	d=0.3 g, 90 min, Co =100 mg/L	>95%	This study

Co= Initial concentration, t=contact time, d=Adsorbent dosage, pH, T=temperature

Table 4. *Thermodynamics parameters for Zn^{2+}, Pb^{2+} and Cu^{2+} adsorption onto the Ag/clay*

Adsorbate	**ΔH° (kJ/mol)**	**ΔS° (kJ/mol.K)**	**ΔG° (kJ/mol)**			**R^2**
			303K	**313K**	**323K**	
Zn^{2+}	-59.986	$-2.562x10^{-3}$	-2.071	-3.877	-6.082	0.999
Pb^{2+}	-28.101	$8.384\ x10^{-2}$	-1.007	-1.866	-2.890	0.998
Cu^{2+}	-70.46	$2.119\ x10^{-1}$	-2.136	-3.929	-6.821	1.000

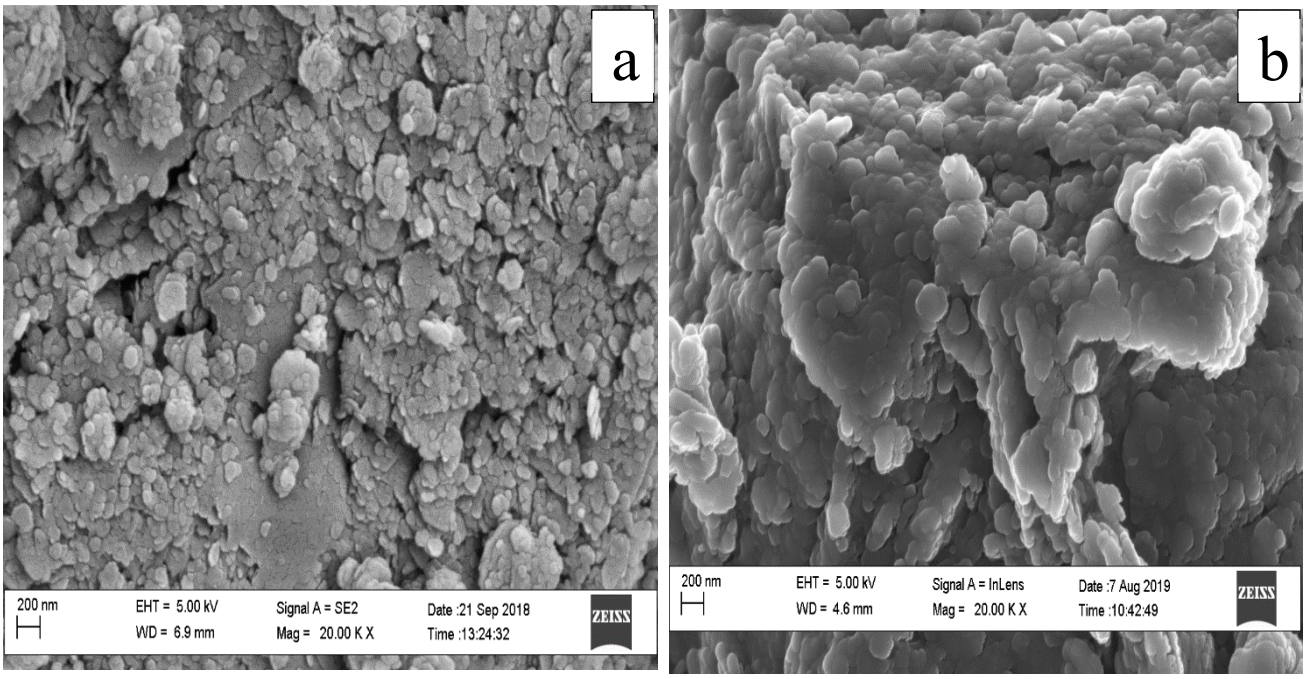

Figure 4. SEM Image of (a) Raw clay (b) Silver/clay adsorbent

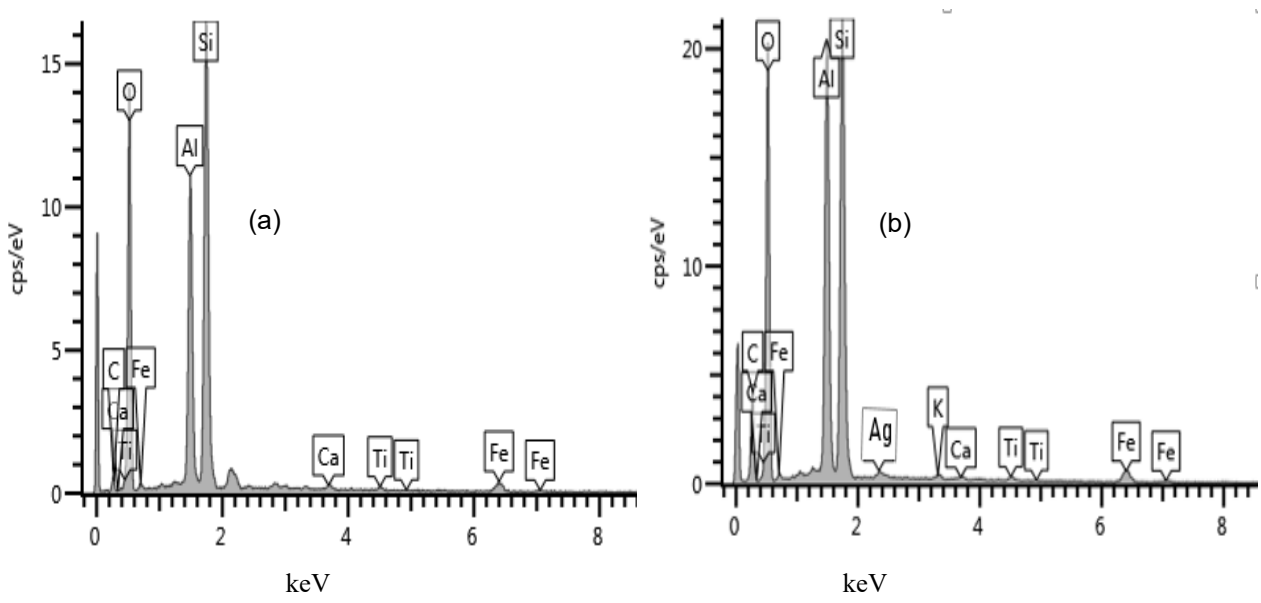

Figure 5. EDS of the (a) Raw-clay and (b) Silver-Clay Adsorbents

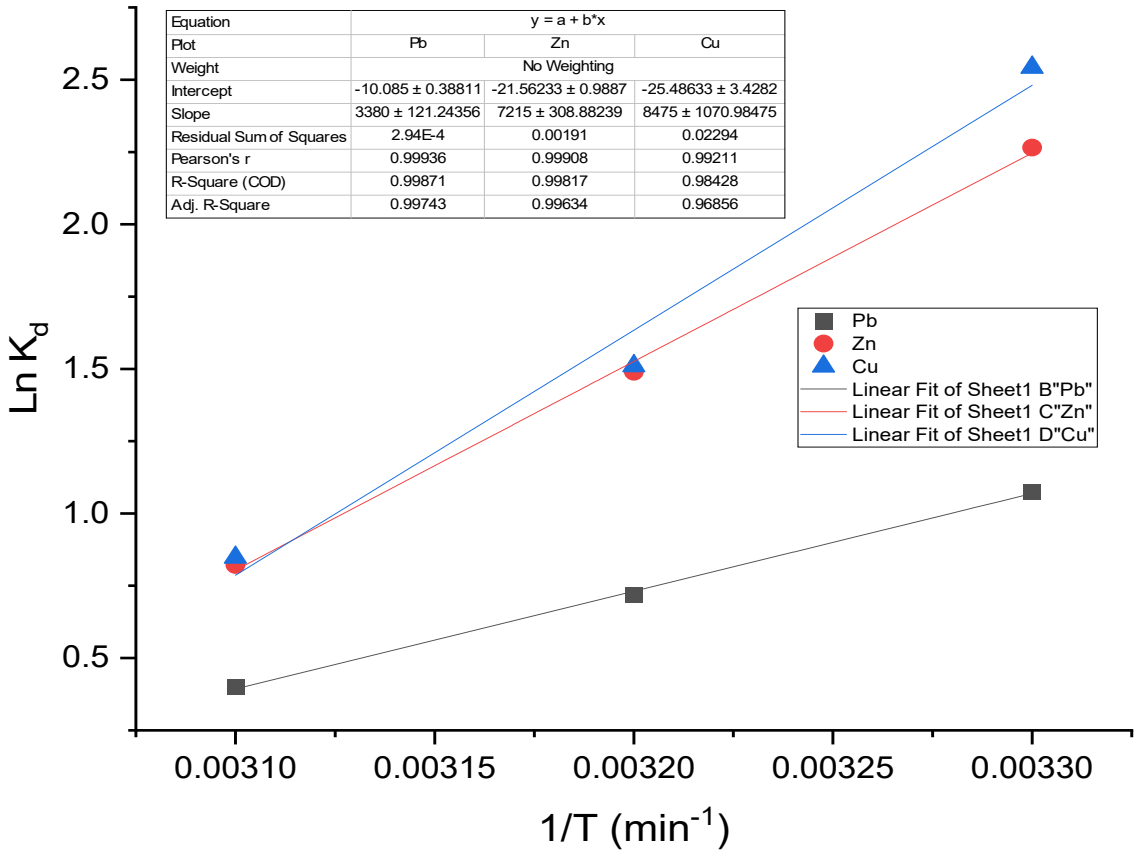

Figure 12. *Vant Hoff"s plot for Zn^{2+}, $Pb^{2+,}$ and Cu^{2+} adsorption onto the Ag/clay*